First-Stokes and second-Stokes multi-wavelength continuous-wave operation in Nd:YVO_4/$BaWO_4$ Raman laser under in-band pumping

Li Fan (樊 莉)*, Xiaoyu Wang (王晓宇), Xiaodong Zhao (赵孝冬), Jianhui Wang (王健辉), Jun Shen (沈 君), Huibo Fan (范会博), Jun Zhu (朱 骏), and Mingya Shen (沈明亚)

College of Physics Science and Technology, Institute of Applied Photonic Technology, Yangzhou University, Yangzhou 225002, China

**Corresponding author: fanli@yzu.edu.cn*

Received May 22, 2020; accepted July 7, 2020; posted online September 17, 2020

A continuous-wave Nd:YVO_4/$BaWO_4$ Raman laser generating simultaneous multi-wavelength first-Stokes and second-Stokes emissions is demonstrated for the first time, to the best of our knowledge. Investigations concerning different pump spot sizes and crystal lengths were conducted to improve the thermal effect and pump absorption. Three first-Stokes lasers at 1103.6, 1175.9, and 1180.7 nm and two second-Stokes lasers at 1145.7 and 1228.9 nm are obtained simultaneously using the Raman shifts of 925 cm^{-1} and 332 cm^{-1} in $BaWO_4$ and 890 cm^{-1} in YVO_4. At the incident pump power of 23.1 W, 1.24 W maximum Raman output power is achieved, corresponding to an optical conversion efficiency of 5.4%. We also present a theoretical analysis of the competition between different Stokes lines.

Keywords: multi-wavelength; intracavity Raman laser; continuous wave; in-band pumping.
doi: 10.3788/COL202018.111401.

Stimulated Raman scattering (SRS) has been recognized as an efficient and flexible method to generate new laser lines that are hard to produce directly for traditional solid-state lasers[1–3]. Furthermore, SRS is a cascaded nonlinear optical process, and there are many different Stokes shift lines in a single Raman crystal, which provides access to generate multi-wavelength emission simultaneously for potential applications in terahertz (THz) radiation generation[4–6], holography, spectral analysis, and laser radar[7]. To date, there have been many investigations on multi-wavelength solid-state Raman lasers operating in both pulsed[8–13] and continuous-wave (CW) regimes[14–21].

For the CW Raman laser, the most efficient configuration is the self-Raman laser, where a single crystal is used as the laser and Raman active medium simultaneously. Since self-Raman lasers have advantages in terms of lower intracavity losses and shorter cavity length, various crystals such as Nd:YVO_4[16], Yb:$KGd(WO_4)_2$ (Yb:KGW)[17], and Nd:KGW[18] have been utilized to generate CW multi-wavelength lasers based on different Stokes shifts and cascaded SRS process. For example, in 2013, Li *et al.* demonstrated a CW self-Raman Nd:YVO_4 laser operating at 1109 nm (the first SRS of 379 cm^{-1}), 1158 nm (the second SRS of 379 cm^{-1}), and 1231 nm (cascaded SRS of 379 cm^{-1} and 893 cm^{-1})[16]. In the case of a simultaneous output of 1109 and 1231 nm Raman lasers, the highest Stokes output power was measured to be 890 mW, corresponding to an optical conversion efficiency of 8.9% with respect to the absorbed pump power. However, the absorbed pump power at 808 nm of this laser was limited to 13 W due to severe thermal effect, which ultimately limited the maximum Raman output powers.

Different from self-Raman configuration, intracavity Raman lasers, where two separate crystals are used for the fundamental and Stokes laser generation, not only reduce the thermal lensing effect but also provide a much wider spectral range of output wavelength by choosing different combinations of laser gain and Raman active media. In 2015, Lee *et al.* demonstrated the generation of CW multiple SRS emissions from an intracavity Nd:YVO_4/$KTiOPO_4$ (KTP) Raman laser. Three Stokes emissions (1095 + 1128 + 1149 nm) were generated simultaneously using shorter Raman shifts of 266 cm^{-1} and 694 cm^{-1} in the KTP crystal (which is beneficial to the generation of multi-wavelength emissions through cascaded SRS due to small quantum defect). However, due to the low Raman gain coefficient of the KTP crystal, the SRS output power was only 0.56 W at 15 W pump power, and the corresponding optical conversion efficiency was only 3.7%[19]. Among the commonly known Raman crystals, the $BaWO_4$ crystal is regarded as an excellent SRS medium due to its high Raman gain (8.5 cm/GW at 1064 nm pump for the 925 cm^{-1} Raman shift). Moreover, besides the primary Stokes shift of 925 cm^{-1}, the $BaWO_4$ crystal also possesses other Stokes shifts such as 332 cm^{-1} and 797 cm^{-1}, which are conducive to generating multi-wavelength Raman lasers. Multi-wavelength $BaWO_4$ Raman lasers have been well investigated in the pulsed regime[22–29]. However, with regard to the CW operation, only in 2012, Li *et al.* reported a Nd:YVO_4/$BaWO_4$ low-power multi-wavelength Raman laser system. In Li's work, three first-Stokes lines at 1176, 1103, and 1180 nm, which are the first SRS of 890 cm^{-1} in Nd:YVO_4 and first SRS of 332 cm^{-1} and 925 cm^{-1} in $BaWO_4$ from a 1064 nm

fundamental laser, were observed simultaneously. Finally, they overcame the SRS competition of undesirable Stokes lines (1176 and 1103 nm) and generated pure CW yellow output of 194 mW at 590 nm for just 3.8 W pump power[15]. Owing to low pump power, no second-Stokes emission is detected. Hence, although higher-order multi-wavelength Raman lasers based on the $BaWO_4$ crystal have been demonstrated in the Q-switched regime[24,28,29], the CW operation has not been realized successfully so far.

In this Letter, simultaneous CW multi-wavelength first-Stokes and second-Stokes emissions are generated in a $Nd:YVO_4/BaWO_4$ intracavity Raman laser for the first time, to the best of our knowledge. To improve thermal effect and pump absorption, an 879 nm wavelength-locked laser diode (LD) is used as the in-band pumping source. Then, higher-order Stokes emissions via the cascading SRS process are generated with the aid of thoughtful resonator design. The optimization entails minimizing thermal effect through an increase of pump spot size, maximizing pump absorption through an increase of crystal length, and maximizing intracavity fundamental power density through minimization of cavity mode size. Finally, when a 1:3 coupler and a 20-mm-long composite crystal are used, five CW Stokes lines at 1103.6 nm (the first Stokes of 332 cm^{-1} in $BaWO_4$), 1145.7 nm (the second Stokes of 332 cm^{-1}), 1175.9 nm (the first Stokes of 890 cm^{-1} in YVO_4), 1180.7 nm (the first Stokes of 925 cm^{-1} in $BaWO_4$), and 1228.9 nm (cascaded SRS of 332 cm^{-1} and 925 cm^{-1}) can be generated simultaneously. An output power of multi-wavelength Raman lasers up to 1.24 W was obtained under 23.1 W incident pump power, and the corresponding optical conversion efficiency was 5.4%. Besides, the competition among different Raman vibrational modes has been investigated in this high power system. These laser wavelengths expand the range of output wavelengths of the $Nd:YVO_4/BaWO_4$ Raman laser and are expected to find applications in areas like spectral analysis, laser radar, and THz generation.

The experimental setup of the CW $Nd:YVO_4/BaWO_4$ Raman laser is shown in Fig. 1. A 30 W, 879 nm wavelength-locked fiber-coupled LD (nLIGHT, Inc.), having a core diameter of 200 μm and a numerical aperture of 0.22, was used as the pump source. As we know, in-band pumping has been proved to be an effective method to reduce the heat load. However, for the $Nd:YVO_4$ crystal, the absorption coefficient at 879 nm is smaller than that at the 808 nm conventional pump, which results in the lower pump absorption and restrains the efficiency improvement. Therefore, the emission spectrum of the pump diode in our work was narrowed and locked to the absorption band of the $Nd:YVO_4$ crystal around 879 nm with spectral linewidth of less than 0.3 nm (full width at half-maximum, FWHM) in order to mitigate the thermal effect and simultaneously improve the pump absorption. In order to avoid crystal damage and reduce thermal effect, two commercial couplers with different magnifications (1:2 and 1:3) were used to expand and focus the pump light into the laser crystals. The pump spot diameters in the laser crystals were approximately 400 and 600 μm, respectively.

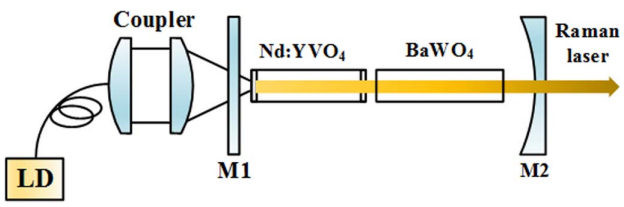

Fig. 1. Schematic diagram of the CW multi-wavelength $Nd:YVO_4/BaWO_4$ intracavity Raman laser.

In order to relieve the thermal lensing effect, two a-cut composite $YVO_4/Nd:YVO_4/YVO_4$ crystals (Crystech, Inc.), 0.3% (atomic fraction)-doped $Nd:YVO_4$ with two 2-mm-long pure YVO_4 diffusion-bounded at the two end facets, were used as the laser medium. Two crystal dimensions of 4 mm × 4 mm × 14 mm and 4 mm × 4 mm × 20 mm were chosen to optimize the pump absorption. All the laser crystals were anti-reflection (AR) coated at 800−1600 nm ($R < 5\%$@879 nm, $R < 0.5\%$@1064 nm, and $R < 0.2\%$@1180 nm). The Raman active medium was a b-cut $BaWO_4$ crystal with a dimension of 4 mm × 4 mm × 30 mm, which was AR-coated at 1000–1350 nm ($R < 0.5\%$ at 1064 nm, $R < 0.2\%$ at 1180 nm). All of the laser and Raman crystals were wrapped with indium foil and tightly mounted in water-cooled copper heat sinks with a water temperature of 18°C.

The laser resonator was composed of a flat input mirror M1 and a concave output coupler M2. The performance of the Raman laser was investigated using various output couplers with different radii of curvature (ROCs) (100, 200, 300, 500, and 800 mm). All mirrors were coated with high transmission at 879 nm ($T > 99\%$) and high reflectivity at 1060−1229 nm ($R = 99.89\%$ at 1064 nm, $R = 99.91\%$ at 1103 nm, $R = 99.88\%$ at 1146 nm, $R = 99.8\%$ at 1176−1180 nm, and $R = 98.87\%$ at 1229 nm). The output beams of the fundamental and Raman lasers were separated by two filters (Thorlabs, FEL1100 and FLH1064-8). An optical spectrum analyzer (Yokogawa, AQ-6370C) was used to record the output spectra with a resolution of 0.02 nm.

Firstly, the performance of this CW Raman laser was investigated by using the 1:2 coupler to reimage the pump light into the laser medium, so the spot diameter of pump light incident onto the crystal was approximately 400 μm. A 14-mm-long composite $YVO_4/Nd:YVO_4/YVO_4$ crystal was utilized as the laser medium, and the c axis of the $BaWO_4$ crystal was aligned along the polarization of the fundamental laser to access the higher Raman gain at 925 cm^{-1}[15]. The resonator length was minimized and maintained at ~51 mm. Figure 2(a) shows the optical spectrum of the laser measured under the maximum incident pump power of 26.3 W. We can find that only the fundamental line at 1064.6 nm and the first-Stokes line at 1180.8 nm (corresponding to the 925 cm^{-1} shift in $BaWO_4$) are detected. The spectral linewidths (FWHM)

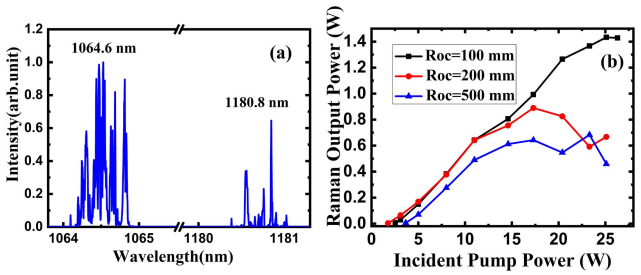

Fig. 2. (a) Output spectrum of the Raman laser with 1:2 coupler and 14 mm crystal under an incident pump power of 26.3 W. (b) Raman output powers with respect to the incident pump power using output couplers with different radii of curvature (100, 200, and 500 mm).

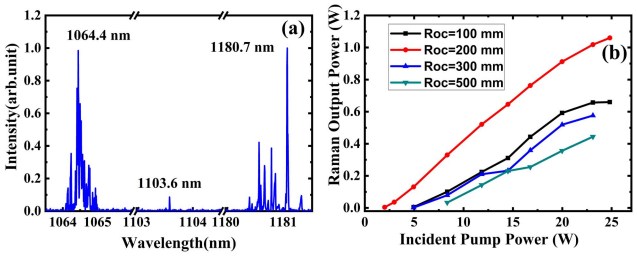

Fig. 3. (a) Output spectrum of the Raman laser with 1:3 coupler and 14 mm crystal at an incident pump power of 24.8 W. (b) Raman output powers with respect to the incident pump power using output couplers with different radii of curvature (100, 200, 300, and 500 mm).

of the two lines were measured to be 0.4 and 0.2 nm, respectively. Figure 2(b) depicts the output power of the Raman laser with respect to the incident pump power using output couplers with different ROCs (100, 200, and 500 mm). As can be seen, the Raman output power is highly dependent on the ROC of the output coupler. The highest output power of the Raman laser was achieved using the output coupler with $R_{oc} = 100$ mm. The Raman threshold was 2.54 W (incident pump power) and the maximum Raman output power of 1.43 W was achieved at an incident pump power of 25.1 W, corresponding to an optical conversion efficiency of 5.7% with respect to the incident pump power and a slope efficiency of 6.3%. It should be noted that the fundamental laser power also grows linearly with the pump power. The output power of the 1064 nm fundamental laser was about 2.1 W at the maximum pump power of 25.1 W, implying that the fundamental laser was not effectively converted to a Raman laser. Besides, it was found that this Raman laser exhibited unstable Raman output due to severe thermal lensing effect, and the Raman output power began to roll over at about 25.1 W pump power for the 100 mm output mirror, whereas this decline was observed at about 17.3 W pump power for the 200 mm and 500 mm output mirrors. This phenomenon validates that the thermal lensing effect on resonator stability can be reduced by using strongly concave output couplers.

Since the thermal lens focal length of the laser medium is proportional to the square of the pump beam radius[30], the 1:2 coupler was replaced by a 1:3 coupler to further relieve the thermal lensing effect. The waist diameter of the pump beam was enlarged to approximately 600 μm. In this case, the output spectrum measured at an incident pump power of 24.8 W, and the Raman output power versus the incident pump power are depicted in Figs. 3(a) and 3(b). We can obviously find that, in addition to the first-Stokes line at 1180.7 nm, the first-Stokes line centered at 1103.6 nm generated by the secondary Raman shift of 332 cm^{-1} in the $BaWO_4$ crystal was also observed. The FWHMs of the fundamental, two first-Stokes lines at 1180.7 and 1103.6 nm were 0.7 nm, 0.5 nm, and 0.02 nm, respectively. The oscillation threshold was 2.01 W and 15 W for the 1180.7 nm and 1103.6 nm Stokes lines, respectively. Different from the above results, for the pump beam diameter of 600 μm, the highest Raman output power was obtained using the output coupler with $R_{oc} = 200$ mm. Under 24.8 W incident pump power, the maximum total Raman output power of 1.08 W was obtained, including the first-Stokes emissions of 0.1 W at 1103.6 nm and 0.98 W at 1180.7 nm. This corresponded to an optical (incident pump power to Stokes) conversion efficiency of 4.4% and a slope efficiency of 4.7%. In this case, the residual fundamental laser output was measured to be 1.3 W, which is lower than 2.1 W in the case of the 1:2 coupler, indicating that conversion efficiency from the fundamental to the Stokes optical field is improved. However, the Raman output power and diode-to-Stokes conversion efficiency are slightly lower than those obtained by the 400 μm pump spot. This could be attributed to the competition between different Stokes transitions, which has a considerably negative impact on laser performance[15,16,18]. Note that the output power increased linearly as pump power increased, and the rollover in Raman output power was not observed, showing that the thermal effect had been effectively improved by increasing the pump spot.

Based on the ABCD matrix resonator model, we simulated the TEM_{00} mode sizes of the fundamental laser on the entrance facet of the laser crystal, in relation to the incident pump power under different pump spots and output couplers with different ROCs (100 and 200 mm), as depicted in Fig. 4. It can be seen that the use of an output mirror with a smaller curvature radius can generate a smaller fundamental mode size inside the cavity, which results in higher Raman conversion efficiency[31] for the output mirror with $R_{oc} = 100$ mm in Fig. 2(b). However, for pump spot radius of 200 μm, the cavity mode size varies dramatically with pump power because thermal lensing effect becomes strong as pump power increases. When the incident pump power increases to 22 W, the mode radius of fundamental laser increases to more than 200 μm, and the resonator cannot satisfy the stable-cavity condition, leading to a decline of Raman output power as shown in Fig. 2(b). For the larger pump spot radius of 300 μm, the resonator maintains cavity stability in the whole

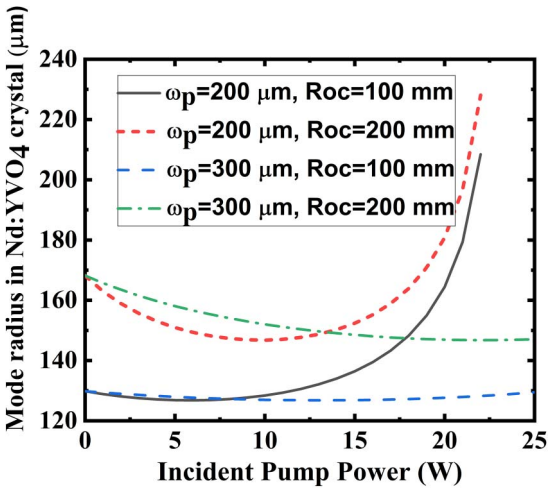

Fig. 4. Simulated cavity mode sizes of the fundamental laser in the $Nd:YVO_4$ laser crystal as a function of incident pump power under different pump spots for output couplers with different radii of curvature (100 and 200 mm).

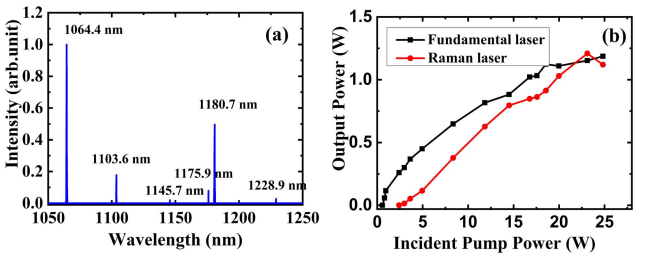

Fig. 5. (a) Output spectrum of the Raman laser with 1:3 coupler and 20 mm crystal under an incident pump power of 23.1 W. (b) Output powers of the fundamental and Raman lasers with respect to the incident pump power.

pump power range and the change in mode size is relatively small, which results in a relatively stable Raman laser output, as shown in Fig. 3(b). In this case, the relatively larger fundamental mode size in the laser crystal generated by the 200 mm R_{oc} output mirror (compared to 100 mm R_{oc} output mirror) achieves better mode matching with the spot size of pump beam, leading to a higher Raman output power. Moreover, it is worth mentioning that when a 10-mm-long conventional $Nd:YVO_4$ laser crystal was used in this system (pumped by 879 nm LD) or the 14-mm-long $YVO_4/Nd:YVO_4/YVO_4$ composite crystal was end-pumped by an 808 nm LD, only the Stokes line at 1180 nm was generated. This indicates that the improvement of thermal effect provided by using composite laser crystal, 879 nm LD in-band pumping, and larger pump spot is critically important for achieving simultaneous output of multi-wavelength laser in the CW $Nd:YVO_4/BaWO_4$ Raman laser. Finally, the residual pump power at 879 nm measured through the output coupler was 2.5 W at the maximum pump power of 24.8 W, from which the absorption fraction of this laser crystal was estimated to be only 90%.

To further improve the pump absorption and generate higher-order Stokes emissions, a longer 20-mm composite $YVO_4/Nd:YVO_4/YVO_4$ crystal with 16-mm length of Nd-doped part was used as the laser medium. The resonator length was further lengthened to 54 mm. Figure 5(a) shows the output spectrum of this Raman laser measured under an incident pump power of 23.1 W. In addition to the fundamental laser at 1064.4 nm, five Stokes lines centered at 1103.6, 1145.7, 1175.9, 1180.7, and 1228.9 nm, which correspond to the first and second-Stokes shift of 332 cm^{-1} in $BaWO_4$, first-Stokes shift of 890 cm^{-1} in $Nd:YVO_4$, first-Stokes shift of 925 cm^{-1} in $BaWO_4$, and cascaded Stokes shift of 925 cm^{-1} and 332 cm^{-1} in $BaWO_4$, respectively, were observed simultaneously. The threshold pump powers for the fundamental laser and five Stokes lasers at 1180.7, 1175.9, 1103.6, 1228.9, 1145.7 nm were 0.08, 2.4, 3.6, 17.4, 17.6, and 18.6 W, respectively. As the pump power increased, noticeable spectral broadening of the fundamental laser was observed. The fundamental linewidth was approximately 0.14 nm at the Raman threshold of 2.4 W and increased to 0.56 nm at the maximum pump power of 24.8 W, which will reduce the effective Raman gain and limit the Raman conversion efficiency[32–34]. As far as we know, this is the first time that simultaneous output of first Stokes at 1180.7 and 1103.6 nm, second Stokes at 1145.7 nm, and cascaded Stokes at 1228.9 nm is observed within a CW $Nd:YVO_4/BaWO_4$ intracavity Raman laser.

For the 20-mm-long crystal, the highest output power of Raman laser was still obtained when the output mirror with 200 mm R_{oc} was used. Figure 5 (b) shows the output power of the fundamental laser and five Stokes lasers in relation to the incident pump power. Under the incident pump power of 23.1 W, the highest Raman output power was 1.24 W – containing 0.28, 0.03, 0.12, 0.77, and 0.04 W Raman output powers at 1103.6, 1145.7, 1175.9, 1180.7, and 1228.9 nm, respectively, which were estimated from the relative individual intensity of the output spectrum in Fig. 5(a). This corresponds to a total optical conversion efficiency of 5.4% and a slope efficiency of 6.0%. We can find that the Raman output power and conversion efficiency are slightly higher than the results of 14 mm composite crystal. However, the roll-over phenomenon in Raman output power appeared again as the pump power exceeded 23.1 W, which was attributed to the strong thermal lensing induced by the additional generation of the second-Stokes emissions and relatively longer cavity length. In addition, it is worth noting that the fluctuation of Raman output power was also more evident, and the output power fluctuation within 30 min was measured to be 3.5%, which is caused by the competition between different Raman lines. Under the maximum incident pump power of 24.8 W, the residual pump power at 879 nm was measured to be 0.865 W, and the corresponding absorption fraction of laser crystal was raised to 96.5%. These results demonstrate that long crystal can significantly improve the pump absorption, resulting in higher fundamental laser power, which is conducive to

the simultaneous generation of multi-wavelength Raman lasers. Based on all the above experimental results, the simultaneous multi-wavelength output in the CW Nd:YVO_4/$BaWO_4$ Raman laser is mainly due to lower thermal effect and higher pump absorption which were obtained by using wavelength-locked 879-nm LD, larger pump spot, and longer laser crystal.

Compared with other multi-wavelength CW Raman lasers with Nd-doped crystal[16,18,19], the output powers achieved in this work are relatively higher. Although the conversion efficiency is lower than that of Nd:YVO_4 self-Raman laser[16] due to higher cavity losses, it is higher than that of Nd:YVO_4/KTP intracavity Raman laser[19]. This is achieved by the combination of using a longer composite YVO_4/Nd:YVO_4/YVO_4 laser crystal, a $BaWO_4$ Raman crystal with higher Raman gain, and improved thermal management by using an 879 nm LD and a larger pump spot. In addition, it can be observed from Fig. 5(b) that the fundamental output power also increases linearly as pump power increases. At the maximum pump power of 24.8 W, 1.187 W output power at the fundamental wave (1064.4 nm) was measured, indicating that the reflectivity of the output coupler at 1064 nm was not at its optimum. In addition, given that reflectivity of the input mirror and output mirror is the same, the Raman laser also has an output through the input mirror. However, only the Raman output power after the output mirror is measured in this work. Hence, notable improvements in Raman output power and conversion efficiency can be anticipated by increasing the reflectivity of the cavity mirror at the fundamental wavelength while simultaneously optimizing the coating of the input mirror.

Finally, we investigated the competition between different Raman shifts in this laser system. According to Ref. [18,31], the threshold pump power for Raman laser can be estimated by the formula

$$P_p = \frac{A_R}{g_R l_R}\frac{\lambda_F}{\lambda_P}\frac{(T_S + L_S)(T_F + L_F)}{2}.$$

Since other parameters are approximately equal for different Stokes lines, it is evident that the threshold pump power is proportional to the value of $\frac{A_R}{g_R l_R}$, where g_R is the Raman gain coefficient, l_R is the Raman crystal length, and A_R is the spot area of the transverse electromagnetic (TEM_{00}) fundamental mode in the Raman medium. Thus, we can take the parameter $\kappa_R = g_R l_R / A_R$ to evaluate the competition between different Stokes emissions, as discussed in Ref. [15]. For different Stokes shifts, the larger the value of parameter κ_R, the more likely oscillation of the corresponding Stokes wavelength is to occur. Considering that the Raman gains for 890 cm^{-1} in Nd:YVO_4 and 925 cm^{-1} in $BaWO_4$ were 4.5 and 8.5 cm/GW, respectively, for the case of 14-mm-long Nd:YVO_4 and 30-mm-long $BaWO_4$, we can estimate that the mode radii in the Nd:YVO_4 and $BaWO_4$ crystals are 154.3 μm and 151.1 μm, respectively. The ratio of $\kappa_{R-BaWO_4}/\kappa_{R-Nd:YVO_4}$ was calculated to be 4.2. For the case of 20-mm-long Nd:YVO_4 and 30-mm-long $BaWO_4$, and using the mode radii of 155.4 μm and 151.1 μm in the Nd:YVO_4 and $BaWO_4$ crystals, the ratio of $\kappa_{R-BaWO_4}/\kappa_{R-Nd:YVO_4}$ was estimated to be 3.0. Therefore, in the latter case, competition between the 1176 nm Stokes line (890 cm^{-1} in Nd:YVO_4) and 1180 nm Stokes line (925 cm^{-1} in $BaWO_4$) is more likely to occur, which is in good agreement with the experimental result reported above.

For the *b*-cut $BaWO_4$ crystal used in our work, the polarization of the fundamental laser delivered by Nd:YVO_4 can be oriented parallel to the *c* or *a* axis of the $BaWO_4$ crystal. According to the spontaneous Raman spectra of the $BaWO_4$ crystal under different polarized pumps in Ref. [15], the Raman gain for the 332 cm^{-1} shift with the *a*-polarized pump was estimated to be 0.92 cm/GW, which was obviously weaker than that of the *c*-polarized pump (3.1 cm/GW). When considering the competition between 925 cm^{-1} and 332 cm^{-1} shifts in $BaWO_4$, the spot area and crystal length are the same, so the value of $\kappa_R^{925}/\kappa_R^{332}$can be calculated to be 2.7 and 9.2 for *c*-polarized and *a*-polarized pumps, which indicates that the competition between 925 cm^{-1} and 332 cm^{-1} in $BaWO_4$ is less likely to occur if the fundamental polarization is aligned along the *a* axis of the $BaWO_4$ crystal. This has been proved in the work[15], but the maximum pump power of that system is only 3.8 W, so it is worth exploring whether the Raman shift related to 332 cm^{-1} can be well suppressed at higher pump power. By rotating the $BaWO_4$ crystal, the polarization of the 1064 nm fundamental laser was changed to be parallel to the *a* axis of $BaWO_4$. To avoid the damage of crystal coating, the maximum pump power was only increased to 20 W. Figure 6(a) shows the output spectrum measured under the pump power of 20 W. It is evident that all Raman emissions related to the 332 cm^{-1} Raman shift (1103.6, 1145.7, and 1228.9 nm) have disappeared, indicating that the Stokes shift of 332 cm^{-1} is completely suppressed at this high pump power system. Figure 6(b) shows the total output power of this Raman laser. The measured thresholds are 2.78 and 2.99 W for 1180.7 nm and 1175.9 nm Raman lasers, respectively. The highest Raman output power was achieved to be 0.96 W at the incident pump power of 20 W, and the corresponding diode-to-Stokes

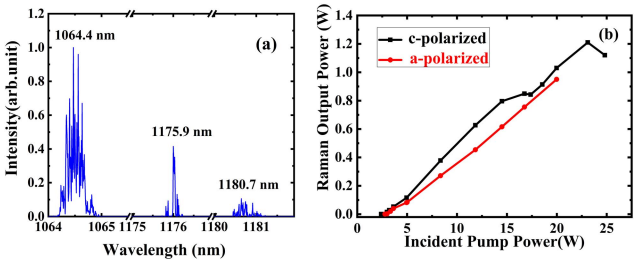

Fig. 6. (a) Output spectrum of the Raman laser with an *a*-polarized pump under incident pump power of 20 W. (b) Raman output powers with respect to the incident pump power when the fundamental polarization is parallel to the *a* axis and *c* axis of $BaWO_4$.

conversion efficiency was 4.8%. For comparison, the Raman output power with the *c*-polarized pump is also depicted in Fig. 6(b). As can be seen, the stability of the output power is greatly enhanced due to the elimination of competition, even though lower output power and higher Raman threshold are obtained for the *a*-polarized pump due to the lower Raman gain.

In summary, we have demonstrated CW operation on five Stokes line outputs from a diode-end-pumped $Nd:YVO_4/BaWO_4$ intracavity Raman laser based on intracavity cascading SRS for the first time, to the best of our knowledge. On the basis of using 879 nm LD in-band pumping and composite laser crystals to improve the thermal effect, we optimize the size of the pump spot and the length of the laser crystal to further reduce thermal effect and improve pump absorption. When the 1:3 coupler (600 μm pump spot) and 20 mm composite laser crystal were used, five Stokes emissions at 1103.6, 1145.7, 1175.9, 1180.7, and 1228.9 nm were generated simultaneously. The total Raman output power reached a maximum of 1.24 W at 23.1 W incident pump power, corresponding to a total optical conversion efficiency of 5.4%. By further optimizing the coating of cavity mirrors, the Raman output power and conversion efficiency can be significantly improved. We also present a theoretical analysis of the competitions between different Stokes lines in $Nd:YVO_4$ and $BaWO_4$ crystals. The results illustrate that it is feasible for generating new multi-wavelength Raman lasers based on intracavity cascading SRS with a $BaWO_4$ crystal in the CW regime. In addition, competition between different Stokes shifts can be successfully controlled by careful selection of the crystal length and orientation. A simultaneous multi-wavelength laser source like this offers more optionality in laser wavelength and may find potential applications in spectroscopy and THz difference-frequency generation.

This work was supported by the National Natural Science Foundation of China (No. 11774301) and the Young Scientists Fund of the National Natural Science Foundation of China (Nos. 11804292 and 61805210).

References

1. C. C. Shen, X. L. Cai, Y. B. Sang, T. C. Zheng, Z. H. Li, D. Liu, W. F. Liu, and J. W. Guo, Chin. Opt. Lett. **18**, 051402 (2020).
2. W. Huang, Y. L. Cui, Z. X. Li, Z. Y. Zhou, and Z. F. Wang, Chin. Opt. Lett. **17**, 071406 (2019).
3. H. S. Wu, J. X. Song, J. Ye, J. M. Xu, H. W. Zhang, J. Y. Leng, and P. Zhou, Chin. Opt. Lett. **16**, 061402 (2018).
4. P. Zhao, S. Ragam, Y. J. Ding, and I. B. Zotova, Opt. Lett. **35**, 3979 (2010).
5. P. Zhao, S. Ragam, Y. J. Ding, and I. B. Zotova, Appl. Phys. Lett. **98**, 131106 (2011).
6. P. Zhao, S. Ragam, Y. J. Ding, and I. B. Zotova, Opt. Lett. **36**, 4818 (2011).
7. M. Wirth, A. Fix, P. Mahnke, H. Schwarzer, F. Schrandt, and G. Ehret, Appl. Phys. B **96**, 201 (2009).
8. X. L. Wang, X. J. Wang, and J. Dong, IEEE J. Quantum Electron. **24**, 1400108 (2018).
9. W. Jiang, Z. Li, S. Q. Zhu, H. Yin, Z. Q. Chen, G. Zhang, and W. D. Chen, Opt. Express **25**, 14033 (2017).
10. J. H. Guo, H. Y. Zhu, Y. M. Duan, C. W. Xu, X. K. Ruan, G. H. Cui, and L. F. Yan, J. Opt. **19**, 035501 (2017).
11. H. Y. Lin, X. H. Huang, D. Sun, and X. Liu, J. Mod. Opt. **63**, 2235 (2016).
12. Y. M. Duan, J. Zhang, H. Y. Zhu, Y. C. Zhang, C. W. Xu, H. Y. Wang, and D. Y. Fan, Opt. Lett. **43**, 4550 (2018).
13. J. P. Lin and H. M. Pask, Opt. Express **20**, 15180 (2012).
14. J. J. Neto, J. P. Lin, N. U. Wetter, and H. Pask, Opt. Express **20**, 9841 (2012).
15. X. L. Li, A. J. Lee, Y. J. Huo, H. J. Zhang, J. Y. Wang, J. A. Piper, H. M. Pask, and D. J. Spence, Opt. Express **20**, 19305 (2012).
16. R. Li, R. Bauer, and W. Lubeigt, Opt. Express **21**, 17745 (2013).
17. M. T. Chang, W. Z. Zhuang, K. W. Su, Y. T. Yu, and Y. F. Chen, Opt. Express **21**, 24590 (2013).
18. C. Y. Tang, W. Z. Zhuang, K. W. Su, and Y. F. Chen, IEEE J. Quantum Electron. **21**, 1400206 (2015).
19. C. Y. Lee, C. C. Chang, C. L. Sung, and Y. F. Chen, Opt. Express **23**, 22765 (2015).
20. X. L. Wang, J. Dong, X. J. Wang, J. Xu, K. I. Ueda, and A. A. Kaminskii, Opt. Lett. **41**, 3559 (2016).
21. Y. F. Chen, Y. Y. Pan, Y. C. Liu, H. P. Cheng, C. H. Tsou, and H. C. Liang, Opt. Express **27**, 2029 (2019).
22. M. Frank, S. N. Smetanin, M. Jelinek, D. Vyhlidal, L. I. Ivleva, P. G. Zverev, and V. Kubecek, Opt. Lett. **43**, 2527 (2018).
23. M. Frank, M. Jelínek, Jr., D. Vyhlidal, V. Kubecek, L. I. Ivleva, P. G. Zverev, and S. N. Smetanin, Laser Phys. **28**, 025403 (2018).
24. H. B. Shen, Q. P. Wang, X. Y. Zhang, X. H. Chen, F. Bai, Z. J. Liu, L. Gao, Z. H. Cong, Z. G. Wu, W. T. Wang, Y. G. Zhang, W. X. Lan, and C. Wang, Opt. Lett. **37**, 4519 (2012).
25. H. B. Shen, Q. P. Wang, X. Y. Zhang, Z. J. Liu, F. Bai, X. H. Chen, Z. H. Cong, L. Gao, Z. G. Wu, W. T. Wang, W. X. Lan, and C. Wang, Appl. Phys. Express **5**, 112704 (2012).
26. H. B. Shen, Q. P. Wang, P. Li, G. P. Lv, X. Y. Zhang, Z. J. Liu, X. H. Chen, Z. H. Cong, L. Gao, X. T. Tao, H. J. Zhang, and J. X. Fang, Opt. Commun. **306**, 165 (2013).
27. Y. Liu, Z. J. Liu, Z. H. Cong, Y. F. Li, J. B. Xia, Q. M. Lu, S. S. Zhang, and S. J. Men, Opt. Express **22**, 21879 (2014).
28. H. B. Shen, Q. P. Wang, X. Y. Zhang, X. H. Chen, Z. H. Cong, Z. G. Wu, F. Bai, W. X. Lan, and L. Gao, Opt. Express **20**, 17823 (2012).
29. H. N. Zhang, X. H. Chen, Q. P. Wang, and P. Li, Laser Phys. Lett. **11**, 105806 (2014).
30. M. E. Innocenzi, H. T. Yura, C. L. Fincher, and R. A. Fields, Appl. Phys. Lett. **56**, 1831 (1990).
31. D. J. Spence, P. Dekker, and H. M. Pask, IEEE J. Quantum Electron. **13**, 756 (2007).
32. G. M. Bonner, J. P. Lin, A. J. Kemp, J. Y. Wang, H. J. Zhang, D. J. Spence, and H. M. Pask, Opt. Express **22**, 7492 (2014).
33. Q. Sheng, A. Lee, D. Spence, and H. Pask, Opt. Express **26**, 32145 (2018).
34. Q. Sheng, R. Li, A. J. Lee, D. J. Spence, and H. M. Pask, Opt. Express **27**, 8540 (2019).